LETTER

doi:10.1038/nature10685

Forcing of wet phases in southeast Africa over the past 17,000 years

Enno Schefuß[1], Holger Kuhlmann[1], Gesine Mollenhauer[1,2], Matthias Prange[1] & Jürgen Pätzold[1]

Intense debate persists about the climatic mechanisms governing hydrologic changes in tropical and subtropical southeast Africa since the Last Glacial Maximum, about 20,000 years ago. In particular, the relative importance of atmospheric and oceanic processes is not firmly established[1–5]. Southward shifts of the intertropical convergence zone (ITCZ) driven by high-latitude climate changes have been suggested as a primary forcing[2,3], whereas other studies infer a predominant influence of Indian Ocean sea surface temperatures on regional rainfall changes[4,5]. To address this question, a continuous record representing an integrated signal of regional climate variability is required, but has until now been missing. Here we show that remote atmospheric forcing by cold events in the northern high latitudes appears to have been the main driver of hydro-climatology in southeast Africa during rapid climate changes over the past 17,000 years. Our results are based on a reconstruction of precipitation and river discharge changes, as recorded in a marine sediment core off the mouth of the Zambezi River, near the southern boundary of the modern seasonal ITCZ migration. Indian Ocean sea surface temperatures did not exert a primary control over southeast African hydrologic variability. Instead, phases of high precipitation and terrestrial discharge occurred when the ITCZ was forced southwards during Northern Hemisphere cold events, such as Heinrich stadial 1 (around 16,000 years ago) and the Younger Dryas (around 12,000 years ago), or when local summer insolation was high in the late Holocene, that is, during the past 4,000 years.

Climate changes reconstructed from sediments in Lake Malawi, the southernmost of the East African great lakes and located within the Zambezi catchment, point to arid conditions and strong northerly wind anomalies during Northern Hemisphere cold events, such as the Younger Dryas[2,3]. It has been inferred that these periods represent southward shifts of the ITCZ[2,3,6]. Dry conditions during the Younger Dryas and Heinrich stadial 1 (HS1) in Lake Tanganyika, located closer to the Equator in East Africa, were interpreted to have been caused by lowered Indian Ocean sea surface temperature[4] (SST). Recently, widespread drought conditions during HS1 in East Africa have similarly been suggested to be driven by cold conditions in the Indian Ocean[5]. Such interpretations are based on meteorological observations that modern rainfall in eastern and southern Africa is strongly related to high SST in the western and southwestern Indian Ocean, respectively[7]. In contrast, Lake Chilwa—located southeast of Lake Malawi—recorded high-stands, which appear to be solely associated with Northern Hemisphere cold events[8]. Further westward in the interior of subtropical southern Africa, palaeo-environmental information is sparse. Age dating of dunes in western Zambia and western Zimbabwe points to dry conditions at 18,000–17,000, 15,000–14,000, 11,000–8,000 and 6,000–4,000 years before present (yr BP; ref. 9), implying that non-dune-building periods around 16,000 yr BP and from 13,000 to 12,000 yr BP roughly correspond to the wet periods found at Lake Chilwa[8]. Palaeo-shorelines and other geomorphologic evidence from the Central Kalahari point to the existence of an extended lake system around the time of HS1 and around 8,500 yr BP, with evidence for the existence of smaller lakes around the time of the Younger Dryas[10]. It thus appears that the climatic history of subtropical southern Africa is complex, and the importance of the various potential climatic forcing mechanisms remains unresolved.

To provide more insights into the climatic forcing of hydrology and land–ocean linkages in southeast Africa, we present a reconstruction of precipitation changes in the Zambezi catchment and its sedimentary discharge fluctuations in conjunction with SST estimates of the southwest Indian Ocean. The Zambezi catchment is located at the southern boundary of the present-day seasonal ITCZ migration, and is thus ideally suited to have recorded past changes in its southward extension. Under modern conditions, austral summer rainfall associated with the ITCZ extends to 15–20° S (ref. 6; Fig. 1a, b). A low-pressure cell forms over southern Africa during summer; it attracts

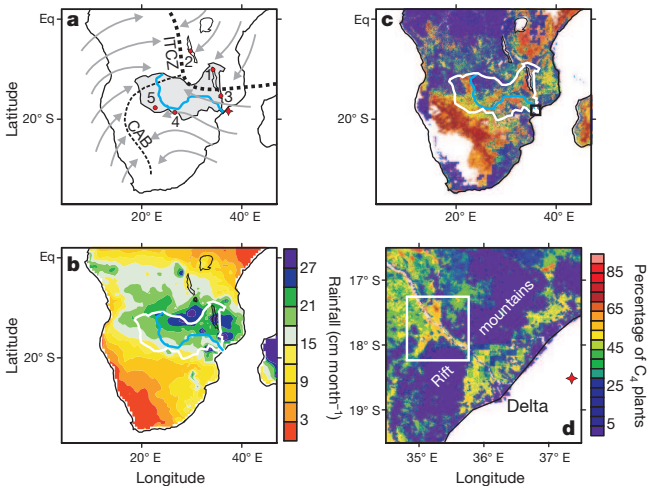

Figure 1 | Modern atmospheric circulation over southern Africa during Southern Hemisphere summer, summer rainfall and vegetation types. **a**, Schematic representation of the atmospheric circulation over southern Africa during austral summer (December, January, February; DJF) with approximate position of the ITCZ and the Congo Air Boundary (CAB). Indicated are: the main course of the Zambezi River (blue), the Zambezi catchment (grey) and the location of GeoB9307-3 (red diamond). Filled red circles indicate locations of other records discussed in the text: (1) Lake Malawi[2], (2) Lake Tanganyika[4], (3) Lake Chilwa[8], (4) dunes in Zambia and Zimbabwe[9], and (5) palaeo-shorelines in the Kalahari[10]. **b**, Austral summer (DJF) rainfall for the period 1950–99 (University of Delaware data set; http://www.esrl.noaa.gov/psd/data/gridded/data.UDel_AirT_Precip.html). Outline of the Zambezi catchment in white and main course of the Zambezi River in blue. **c**, Modern-day vegetation type distribution[15], shown as percentage of C_4 plants. White areas are either >95% C_4 or not vegetated. Zambezi catchment and Zambezi River as in **b**. Colour scale as in **d**. Black box indicates the area shown in **d**. **d**, Map of the relative C_4 plant abundance[15] in the lower Zambezi catchment. White areas are not vegetated. White box indicates the location of the lower Zambezi floodplain.

[1]MARUM – Center for Marine Environmental Sciences and Faculty of Geosciences, University of Bremen, D-28359 Bremen, Germany. [2]Alfred Wegener Institute for Polar and Marine Research, D-27568 Bremerhaven, Germany.

moisture from the tropical Atlantic by tropical westerly air flow, and from the Indian Ocean by easterly air flow[6]. Atlantic moisture influences are restricted to the highlands south of the Congo basin, separated by the Congo Air Boundary from the majority of subtropical southern Africa that receives moisture from the Indian Ocean[11]. During austral winter, a high-pressure system over southern Africa leads to dry conditions, except in a small winter rainfall zone at its southwestern tip[6]. The Zambezi River is the fourth-largest river in Africa, originating in Zambia and flowing southeastward to the Indian Ocean. The upper Zambezi is separated from its lower part by the Victoria Falls. After flowing through a series of gorges, the river enters a broad valley and spreads out over a large floodplain in its lower part. About 150 km from the coast, the catchment narrows where the river flows through the eastern Rift mountains. Maximum rainfall in the catchment during the peak of the southward ITCZ migration occurs in this area[12] (Fig. 1b), periodically causing extensive flooding[13]. The floodplain is dominated by papyrus swamps (dominated by *Cyperus papyrus*, a C_4 plant) with a lower importance of reed swamps (*Phragmites* and *Typha*, C_3 plants)[14]. The C_4 plant dominance in the lower Zambezi floodplain is seen in the relative abundance of C_4 plants[15] (Fig. 1c, d). Downstream from the Rift mountains, the Zambezi splits up into a flat and wide delta[13]. Woodlands, savannah and extensive mangrove forests (C_3 plants) vegetate the delta and coastal areas[14].

The 6.51-m-long marine sediment core GeoB9307-3 (18° 33.9′ S, 37° 22.8′ E, 542 m water depth) was retrieved about 100 km off the Zambezi delta. The core location is in the zone of high deglacial-Holocene sedimentation of material discharged by the Zambezi River[16]. The chronology of the core is established by 19 ^{14}C AMS (accelerator mass spectrometry) dates on mixed planktonic foraminifera (Supplementary Table 1). On the basis of this chronology, the core covers the past 17,000 years. The average time resolution between the 125 samples is 130 years. For the time periods of HS1 and the Younger Dryas, we detect large increases in sedimentary terrestrial versus marine elemental ratios (Fig. 2b), in relative soil organic matter contributions[17] (branched and isoprenoid tetraether (BIT) index, Fig. 2c), and in sedimentary concentrations of terrestrial-plant-derived long-chain *n*-alkanes (Fig. 2d), indicating enhanced terrestrial discharge by the Zambezi River. The elevated concentrations of *n*-alkanes indicate sustained vegetation cover during HS1 and the Younger Dryas, and decreases of soil pH estimates during these intervals (Supplementary Fig. 4) suggest higher rainfall as primary cause. For all these parameters, a slight increase is also detected for the late Holocene compared to the early Holocene. Comparison to records from Lake Malawi[2,3] suggests that the rainfall maximum associated with the ITCZ shifted southward of the Malawi basin during HS1 and the Younger Dryas, causing arid conditions at Lake Malawi while increasing rainfall in the lower Zambezi catchment. The stronger increases in these discharge-related parameters during the Younger Dryas and HS1 compared to the late Holocene points to the influence of sea-level changes. Sea level was reduced during the last deglaciation[18], resulting in a more proximal location of the Zambezi outflow to the core site.

In order to investigate the continental hydrologic changes without the influence of sea-level changes, we analysed the hydrogen isotope composition of lipid biomarkers derived from higher plants. Hydrogen isotope compositions of the *n*-C_{31} alkane range from −136‰ to −164‰ (relative to the VSMOW standard), showing depleted values from 16,950 to 14,700 yr BP, corresponding to the period of HS1, and from 12,800 to 11,350 yr BP, representing the Younger Dryas period (Fig. 2e). The most enriched values are found in the early Holocene, followed by a gradual decline towards the late Holocene that is interrupted by several short-term excursions to more enriched values. The *n*-C_{31} alkane derives from the protective wax coating of leaves of terrestrial higher plants[19]. Its hydrogen isotope composition reflects changes in the isotopic composition of precipitation, with potential enrichment due to evaporation from soils and evapo-transpiration from leaves[20], which amplify the recorded signal under arid conditions[21]. In monsoonal regions, depleted isotopic compositions of precipitation are indicative of changes in the amount of rainfall[22]. These data suggest that changes in rainfall amount caused the discharge pulses detected for the Younger Dryas and HS1.

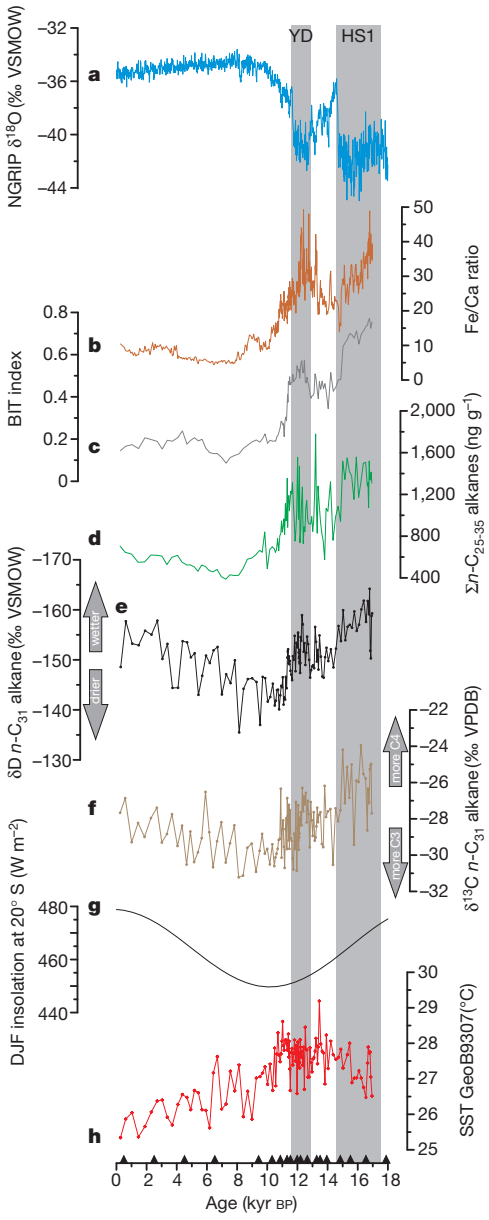

Figure 2 | Records of environmental variability in southeastern Africa over the past 17,000 years. **a**, Oxygen isotope changes in NGRIP ice core[28], mainly reflecting northern high-latitude temperature changes. **b**, Fe/Ca ratio, indicating terrestrial versus marine elemental contributions to sediments of GeoB9307-3. **c**, BIT index of GeoB9307-3, reflecting changes in relative soil organic matter contribution. **d**, Concentrations of long-chain, odd-numbered *n*-alkanes (*n*-C_{25} to *n*-C_{35}) in the sediments of GeoB9307-3. **e**, Hydrogen isotope compositions of the *n*-C_{31} alkane in GeoB9307-3, reflecting rainfall changes in the Zambezi catchment. Error bars based on replicate analyses are shown in Supplementary Fig. 1. **f**, Stable carbon isotope compositions of *n*-C_{31} alkanes in GeoB9307-3, indicating relative contribution changes from the lower Zambezi floodplain. Error bars based on replicate analyses are shown in Supplementary Fig. 2. **g**, Long-term insolation changes over southern Africa (20° S) during Southern Hemisphere summer (DJF)[25]. **h**, TEX_{86}-derived SST record from GeoB9307-3, reflecting ocean temperature changes in the southwest Indian Ocean. Vertical grey bars indicate intervals of Heinrich Stadial 1 (HS1) and the Younger Dryas (YD). Black triangles indicate ^{14}C AMS ages.

Comparison of the δD values of the long-chain plant-waxes with their stable carbon isotope ($\delta^{13}C$) compositions reveals that sedimentary *n*-alkanes with depleted δD values show a stronger C_4 plant signal and vice versa (Fig. 2f). As C_4 plants are usually more drought-tolerant than C_3 plants[23], this correlation is unexpected. Although long-term vegetation changes are not ruled out (see Supplementary Information), the strong coherence of both isotopic signals rather points to a shift in source area associated with the hydrologic changes as the primary cause for the observed relation. We infer that when maximum rainfall and flooding occurs in the floodplain, as under modern-day conditions, more C_4-plant-derived waxes are exported to the ocean, as reflected in the core-top isotopic signature (Figs 1d, 2e). Under more arid conditions, such as during the early Holocene, the export of C_4-plant-derived lipids from the floodplain was diminished, and only low amounts of predominantly C_3-plant-derived waxes from near-coastal vegetation were exported. We thus deduce that the terrestrial signal in core GeoB9307-3 is predominantly derived from the lower Zambezi catchment, dominated by changes in relative contributions from the floodplain. Aeolian transport of terrigenous material from subtropical southern Africa towards the southwest Indian Ocean is negligible, owing to the prevailing easterly winds[12].

Part of the signal seen in the δD record may thus derive from the changes in relative contributions from different vegetation types, seen in the C_3/C_4 changes (see, for example, ref. 24). Although we cannot completely rule out this possible effect, the evidence provided by the other parameters (Fe/Ca ratio, BIT index, *n*-alkane concentrations, soil pH estimates) indicates that the depleted δD values during HS1, the Younger Dryas and the late Holocene indeed reflect increased precipitation in the lower Zambezi catchment.

The long-term trends in the δD and $\delta^{13}C$ records correlate with mean summer insolation (Fig. 2g) over southern Africa[25]: higher insolation intensifies atmospheric convection, leading to higher rainfall over that region[26]. For Heinrich events, modelling results indicate an increase of precipitation associated with isotopically depleted rainfall over southern Africa[27], consistent in magnitude with the isotopic changes detected for HS1. A detailed comparison of the plant-wax isotopic changes with the oxygen isotope changes in the NGRIP ice core[28] (Fig. 3), which reflect northern high-latitude temperature changes, reveals a synchronous onset and end of the Younger Dryas and a synchronous end of HS1. This synchronicity supports our conclusion that the plant waxes are not transported over long distances. As suggested by other studies[8–10], rainfall during HS1 and the Younger Dryas probably also increased in the western parts of the Zambezi catchment. However, plant waxes derived from these more inland parts would carry a much more depleted δD signal due to increased moisture rainout during long-distance transport[29]. We thus infer that long-distance transport of plant waxes by the Zambezi River is of minor importance. Furthermore, the detected synchronicity of isotopic changes suggests a direct forcing of southeast African wet phases by Northern Hemisphere cold events, and points to a large-scale atmospheric teleconnection (see, for example, ref. 30). It is likely that persistent cold conditions in the Northern Hemisphere forced the ITCZ to a more southerly position during these events. The deviations in the amplitudes of isotopic changes of the ice core and the plant waxes during HS1 (Fig. 3) are probably explained by the modulation of rainfall intensity by local insolation.

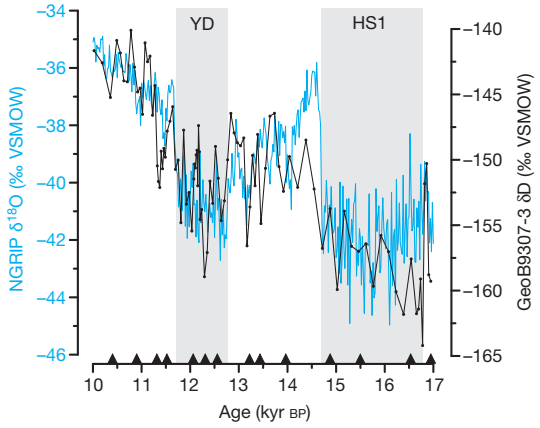

Figure 3 | Detailed comparison of Greenland climate changes with hydrologic variations in the Zambezi catchment during the last deglaciation. Greenland temperature changes reflected in oxygen isotope compositions (blue) of the NGRIP ice core[28] compared to hydrogen isotope changes of the *n*-C_{31} alkane in sediments of GeoB9307-3 reflecting rainfall changes in the Zambezi catchment (black, note inverted scale). Deviations in amplitudes are partly due to modulation of rainfall intensity by local insolation (Fig. 2g). Grey bars and black triangles as in Fig. 2. Error bars based on replicate analyses are shown in Supplementary Fig. 1.

In order to evaluate the effect of southwest Indian Ocean SST changes on continental hydrology, we compare the terrestrial records to a TEX_{86}-based SST record from GeoB9307-3 (Fig. 2h). The TEX_{86} index reflects distributional variations in membrane lipids from marine Thaumarchaeota, related to ocean temperature (see Supplementary Information). The high BIT values in part of the record did not lead to a substantial bias in SST estimates (see Supplementary Information). The SST record shows warm conditions during the Younger Dryas, but does not indicate similarly warm conditions during HS1. Moreover, the timing of SST changes does not correspond to the observed hydrologic changes. Therefore, we suggest that sufficiently warm conditions in the southwest Indian Ocean may have been an important pre-condition for southward movements of the ITCZ and the supply of moisture, but that rainfall changes in the Zambezi catchment over these timescales were not primarily driven by these SSTs. We find no evidence for drought conditions in southeast Africa during HS1 driven by cold conditions in the Indian Ocean[5].

In summary, we conclude that rainfall and discharge changes in the Zambezi catchment result from a combination of local insolation and latitudinal ITCZ shifts, with the latter being directly forced by high-latitude climate changes in the Northern Hemisphere. SST changes in the southwest Indian Ocean appear not to be the primary forcing of past hydrologic changes, but may be an important prerequisite for such changes.

METHODS SUMMARY

Element intensities were measured at 1 cm resolution using a XRF-I core scanner at MARUM, University of Bremen. The central sensor unit is equipped with a molybdenum X-ray source (3–50 keV), a Peltier-cooled PSI detector with a 125 μm beryllium window, and a multichannel analyser with 20 eV spectral resolution. XRF (X-ray fluorescence) data for this study were collected over a 1 cm^2 area using 30 s count time, and conditions of 20 kV and 0.087 mA for the X-ray source.

Sediments were extracted with a Dionex accelerated solvent extractor using dichloromethane:methanol (9:1; v/v). Saturated hydrocarbon fractions were obtained using silica column chromatography by elution with hexane and subsequent elution over $AgNO_3$-coated silica. Squalane was added before extraction as an internal standard. Hydrogen isotope compositions of lipids were analysed on a Trace gas chromatograph coupled via a pyrolysis reactor to a MAT 253 mass spectrometer. Isotope values were measured against calibrated H_2 reference gas. δD values are reported in ‰ versus VSMOW. Further technical information is provided in Supplementary Information.

Compound-specific stable carbon isotope values were analysed on a Trace gas chromatograph coupled via a combustion reactor to a MAT 252 mass spectrometer. Isotope values were measured against calibrated CO_2 reference gas. $\delta^{13}C$ values are reported in ‰ versus VPDB. Further technical information is provided in Supplementary Information.

Polar fractions of the total lipid extracts eluted from silica columns with dichloromethane:methanol (1:1; v/v) were filtered through a 4-μm pore size PTFE filter and dissolved in hexane/isopropanol (99:1; v/v) before analysis by high performance liquid chromatography/atmospheric pressure chemical ionization–mass

spectrometry (HPLC/APCI-MS). An Agilent 1200 series HPLC/APCI-MS system equipped with a Grace Prevail Cyano column (150 mm × 2.1 mm; 3 μm) was used, and separation was achieved in normal phase.

Received 11 May; accepted 27 October 2011.

1. Clement, A. C. & Peterson, L. C. Mechanisms of abrupt climate change of the last glacial period. *Rev. Geophys.* **46,** RG4002 (2008).
2. Johnson, T. C. *et al.* A high-resolution paleoclimate record spanning the past 25,000 years in southern east Africa. *Science* **296,** 113–132 (2002).
3. Castañeda, I. S., Werne, J. P. & Johnson, T. C. Wet and arid phases in the southeast African tropics since the Last Glacial Maximum. *Geology* **35,** 823–826 (2007).
4. Tierney, J. E. *et al.* Northern Hemisphere controls on tropical southeast African climate during the past 60,000 years. *Science* **322,** 252–255 (2008).
5. Stager, C. J., Ryves, D. B., Chase, B. M. & Pausata, F. S. R. Catastrophic drought in the Afro-Asian monsoon region during Heinrich Event 1. *Science* **331,** 1299–1302 (2011).
6. Gasse, F. *et al.* Climatic patterns in equatorial and southern Africa from 30,000 to 10,000 years ago reconstructed from terrestrial and near-shore proxy data. *Quat. Sci. Rev.* **27,** 2316–2340 (2008).
7. Jury, M. R., Enfield, D. B. & Melice, J. L. Tropical monsoons around Africa: stability of El Nino-Southern Oscillation associations and links with continental climate. *J. Geophys. Res.* **107**(C10), 3151, http://dx.doi.org/10.1029/2000JC000507 (2002).
8. Thomas, D. S. G. *et al.* Late Quaternary highstands at Lake Chilwa, Malawi: frequency, timing and possible forcing mechanisms in the last 44 ka. *Quat. Sci. Rev.* **28,** 526–539 (2009).
9. Thomas, D. S. G. & Shaw, P. A. Late Quaternary environmental change in central southern Africa: new data, synthesis, issues and prospects. *Quat. Sci. Rev.* **21,** 783–797 (2002).
10. Burrough, S. L., Thomas, D. S. G. & Singarayer, J. S. Late Quaternary hydrological dynamics in the Middle Kalahari: forcing and feedbacks. *Earth Sci. Rev.* **96,** 313–326 (2009).
11. Gimeno, L. *et al.* On the origin of continental precipitation. *Geophys. Res. Lett.* **37,** L13804, http://dx.doi.org/10.1029/2010GL043712 (2010).
12. Nicholson, S. E. The nature of rainfall variability over Africa on time scales of decades to millennia. *Glob. Planet. Change* **26,** 137–158 (2000).
13. Beilfuss, R. & dos Santos, D. *Patterns of Hydrological Change in the Zambezi Delta, Mozambique* (Working Paper No. 2, International Crane Foundation, Sofala, Mozambique, 2001); available at ⟨http://www.savingcranes.org/images/stories/pdf/conservation/Zambezi_hydrology_Working_Paper2.pdf⟩.
14. Beilfuss, R., Moore, D., Bento, C. & Dutton, P. *Patterns of Vegetation Change in the Zambezi Delta, Mozambique* (Working Paper No. 3, International Crane Foundation, Sofala, Mozambique, 2001); available at ⟨http://www.savingcranes.org/images/stories/pdf/conservation/Zambezi_Vegetation_Working_Paper3.pdf⟩.
15. Still, C. J. & Powell, R. L. in *Understanding Movement, Pattern, and Process on Earth through Isotope Mapping* (eds West, J. B., Bowen, G. J., Dawson, T. E. & Tu, K. P.) 179–194 (Springer, 2010).
16. Schulz, H., Lückge, A., Emeis, K.-C. & Mackensen, A. Variability of Holocene to Late Pleistocene Zambezi riverine sedimentation at the upper continental slope off Mozambique, 15°–21°S. *Mar. Geol.* **286,** 21–34 (2011).
17. Hopmans, E. C., Schefuß, E., Sinninghe Damsté, J. S. & Schouten, S. A novel proxy for terrestrial carbon input based on branched and isoprenoid tetraethers. *Earth Planet. Sci. Lett.* **224,** 107–116 (2004).
18. Fairbanks, R. G. Sea level rise during the last deglaciation as recorded in Barbados corals. *Nature* **342,** 637–642 (1989).
19. Eglinton, G. & Hamilton, R. J. Leaf epicuticular waxes. *Science* **156,** 1322–1335 (1967).
20. Sachse, D., Radke, J. & Gleixner, G. δD values of individual *n*-alkanes from terrestrial plants along a climatic gradient — implications for the sedimentary biomarker record. *Org. Geochem.* **37,** 469–483 (2006).
21. Schefuß, E. Schouten, S. & Schneider, R. R. Climatic controls of Central African hydrology during the last 20,000 years. *Nature* **437,** 1003–1006 (2005).
22. Risi, C., Bony, S. & Vimeux, F. Influence of convective processes on the isotopic composition ($\delta^{18}O$ and δD) of precipitation and water vapor in the tropics: 2. Physical interpretation of the amount effect. *J. Geophys. Res.* **113,** D19306, http://dx.doi.org/10.1029/2008JD009943 (2008).
23. Ehleringer, J. R. & Cerling, T. E. in *Encyclopedia of Global Environmental Change* Vol. 2 (ed. Munn, T.) 186–190 (Wiley & Sons, 2002). pp. 186.
24. Hou, J. Z., D'Andrea, W. J., MacDonald, D. & Huang, Y. S. Hydrogen isotopic variability in leaf waxes among terrestrial and aquatic plants around Blood Pond, Massachusetts (USA). *Org. Geochem.* **38,** 977–984 (2007).
25. Laskar, J. *et al.* A long-term numerical solution for the insolation quantities of the Earth. *Astron. Astrophys.* **428,** 261–285 (2004).
26. Partridge, T. C. *et al.* Orbital forcing of climate over South Africa: a 200,000 year rainfall record from the Pretoria Saltpan. *Quat. Sci. Rev.* **16,** 1125–1133 (1997).
27. Lewis, S. C., LeGrande, A. N., Kelley, M. & Schmidt, G. A. Water vapour source impacts on oxygen isotope variability in tropical precipitation during Heinrich events. *Clim. Past* **6,** 325–343 (2010).
28. Andersen, K. K. *et al.* High-resolution record of Northern Hemisphere climate extending into the last interglacial period. *Nature* **431,** 147–151 (2004).
29. Frankenberg, C. *et al.* Dynamic processes governing lower-tropospheric HDO/H_2O ratios as observed from space and ground. *Science* **325,** 1374–1377 (2009).
30. Broccoli, A. J., Dahl, K. A. & Stouffer, R. J. Response of the ITCZ to Northern Hemisphere cooling. *Geophys. Res. Lett.* **33,** L01702, http://dx.doi.org/10.1029/2005GL024546 (2006).

Supplementary Information is linked to the online version of the paper at www.nature.com/nature.

Acknowledgements This work was supported by the DFG Research Center/Cluster of Excellence 'The Ocean in the Earth System' and DFG grant Sche903/8. Laboratory assistance was provided by K. Siedenberg, M. Segl, W. Bevern, B. Meyer-Schack and R. Kreutz. We thank R. Schneider for logistical support and S. Weldeab for sample preparation for radiocarbon analyses. Comments by Y. Huang and J. Russell improved the manuscript.

Author Contributions Experimental work was carried out by E.S., H.K., G.M. and J.P.; data analysis and interpretation were carried out by E.S., H.K., G.M., M.P. and J.P.

Author Information Data reported here are stored in the Pangaea database (http://www.pangaea.de/10.1594/PANGAEA.771396). Reprints and permissions information is available at www.nature.com/reprints. The authors declare no competing financial interests. Readers are welcome to comment on the online version of this article at www.nature.com/nature. Correspondence and requests for materials should be addressed to E.S. (schefuss@uni-bremen.de).

doi:10.1038/nature10685

Supplementary material

Hydrologic signals in δD compositions of long-chain *n*-alkanes

Long-chain odd-numbered *n*-alkanes, e.g., *n*-C_{27}, *n*-C_{29}, *n*-C_{31} and *n*-C_{33}, are derived from the epi-cuticular wax coating of terrestrial higher plants[1]. Studies of wax lipid distributions of African vegetation[2] suggest that *n*-alkane distributions of rainforest plants (mostly C_3) maximize at the *n*-C_{29} alkane, whereas *n*-alkane distributions of C_3 savannah trees and shrubs and C_4 grasses have their maximum at the *n*-C_{31} alkane[2]. C_4 grasses often show higher amounts of *n*-C_{33} than other savanna plants, however, with substantial variability between investigated taxa[2]. Emergent aquatic plants occurring in the Zambezi floodpain, delta and in coastal areas (e.g., *Cyperus* spp., *Phragmites* spp., *Rhizophora* spp.) have *n*-alkane distributions similar to terrestrial vegetation, typically dominated by longer-chain (>*n*-C_{29}) homologues[3]. In our samples, the *n*-C_{27} alkane could not reliably be isotopically analysed due to its relatively low abundance. The H_3-factor varied from 5.2 to 5.4 over the measuring period. An alkane standard of 15 externally calibrated alkanes was measured every 6 runs. Average absolute deviations from known δD values were consistently < 5 ‰. All samples were run at least in duplicate. Reproducibility for the *n*-C_{29}, the *n*-C_{31}, and the *n*-C_{33} alkane was 1.5 ‰, 1.6 ‰ and 2.2 ‰ on average, respectively. Precision and accuracy of the squalane internal standard were 3.8 and 1.6 ‰, respectively (n=319). Comparison of the δD signals of the *n*-C_{29}, *n*-C_{31} and *n*-C_{33} alkane reveals strong coherence between the *n*-C_{31} and *n*-C_{33} alkane, while the *n*-C_{29} alkane shows less pronounced changes (Fig. S1). The average δD value of all samples decreases from *n*-C_{29} to the *n*-C_{33} (*n*-C_{29}: -148 ± 3 ‰ VSMOW, *n*-C_{31}: -151 ± 5 ‰ VSMOW, *n*-C_{33}: -158 ± 7 ‰ VSMOW) while the total range increases from the *n*-C_{29} to the *n*-C_{33}

(*n*-C_{29}: 21 ‰, *n*-C_{31}: 29 ‰, *n*-C_{33}: 30 ‰). The observed pattern thus suggests that the *n*-C_{31} and *n*-C_{33} alkanes in our samples are derived from more confined plant sources whereas the *n*-C_{29} alkane reflects contributions from a broader range of plant types, e.g., with different growing seasons, growth forms, and sensitivity to soil evaporation and/or evapo-transpiration. Due to the lack of detailed studies on *n*-alkane distributions of plants from the Zambezi catchment, we interpret the δD signal of the *n*-C_{31} alkane as being derived from terrestrial higher plants in general.

Except for the isotopic enrichment due to evaporation in soils and evapo-transpiration from leaves, sedimentary plant waxes mainly record the isotopic composition of precipitation[4]. Several factors might affect changes in isotopic compositions of precipitation in the lower Zambezi catchment[5]. Storage of isotopically depleted water in ice sheets alters the global mean seawater isotopic composition as moisture source of precipitation[5,6]. We did not correct the δD record for seawater isotope changes due to varying ice volume. As global mean seawater was isotopically heavier during the deglaciation than at present[6], such correction would lead to even lighter δD values of plant-waxes during deglaciation and thus lead to more pronounced changes in the records. Water vapour source area changes are ruled out as almost all moisture precipitating over south-east Africa derives from the southwest Indian Ocean[7]. Continental temperature estimates (see below) indicate warmer air temperatures during HS1 and the YD contradicting a temperature effect during these intervals. Changes in the intensity of rainfall[8] and shifts in the location of main rainfall remain as potential drivers of isotopic variability. Higher precipitation rates (amount effect) as well as a shift of main precipitation to an area further inland and/or towards higher altitudes could lead to the observed depleted isotopic compositions during

HS1, the YD and the late Holocene. The relatively small amplitude of the observed δD changes during the YD and HS1 compared to the large gradient in δD compositions of moisture over southern Africa[9], however, rules out a large inland shift of the location of maximum rainfall. In addition, the observed relative synchronicity between the isotopic changes in the NGRIP ice core record and the isotopic changes of the plant waxes argue against a substantial transport distance. We therefore infer that the changes in δD composition of the *n*-C_{31} alkane mainly reflect rainfall intensity changes in the lower Zambezi catchment.

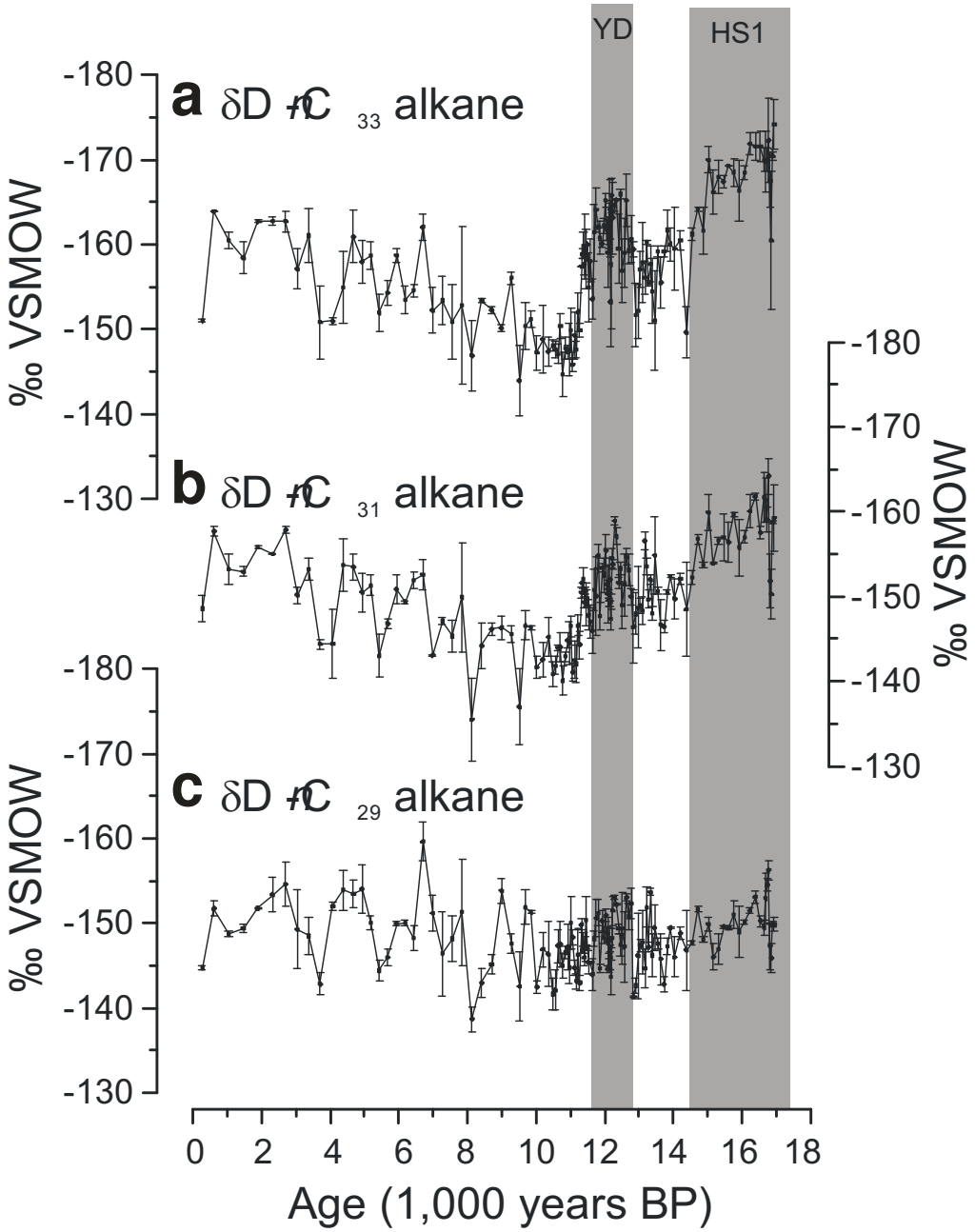

Supplementary Figure S1: Hydrogen isotope compositions of long-chain plant waxes. a, δD of *n*-C_{33} alkane. **b**, δD of *n*-C_{31} alkane. **c**, δD of *n*-C_{29} alkane. Error bars based on replicate analyses. Grey bars indicate intervals of Heinrich Stadial 1 (HS1) and the Younger Dryas (YD).

Vegetation signals in $\delta^{13}C$ compositions of long-chain *n*-alkanes

Stable carbon isotope compositions of plant waxes depend on the type of photosynthetic carbon fixation. Trees, shrubs and bushes use the C_3 pathway, while grasses may utilize either the C_3 or the C_4 pathway[10]. As these carbon fixation pathways lead to distinct carbon isotopic signatures, vegetation sources can be distinguished. $\delta^{13}C$ values of plant wax *n*-alkanes from C_3 plants are around -35.0 ‰ VPDB, while they are around -21.5 ‰ VPDB for C_4 plants[11]. During measurement an alkane standard of 12 externally calibrated alkanes was measured every 6 runs. Average absolute deviations from known $\delta^{13}C$ values were consistently < 0.5 ‰. All samples were run at least in duplicate. Reproducibility for the *n*-C_{29} and the *n*-C_{33} alkane was 0.3 ‰ on average and 0.2 ‰ on average for the *n*-C_{31} alkane. Precision and accuracy of the squalane internal standard were 0.6 and 0 ‰, respectively (n=334). The average $\delta^{13}C$ values of the *n*-C_{29} (-28.9 ± 1.3 ‰ VPDB) and *n*-C_{31} alkane (-28.3 ± 1.5 ‰ VPDB) are similar, while the *n*-C_{33} alkane is more ^{13}C-enriched (-26.8 ± 1.8 ‰ VPDB), indicating that it contains a higher relative C_4 plant contribution (Fig. S2). Additionally, variability increases from the *n*-C_{29} to the *n*-C_{33} (*n*-C_{29}: 6.6 ‰, *n*-C_{31}: 7.3 ‰, *n*-C_{33}: 8.1 ‰). Again, this indicates that the *n*-C_{29} alkanes are derived from more stable woody C_3 plant sources, while the *n*-C_{31} and *n*-C_{33} alkanes contain higher contributions from C_4 plants (tropical grasses and sedges) at certain times. It has been found different plant types differ substantially in their hydrogen isotope fractionation[12]. Since there is, however, yet large uncertainty about apparent hydrogen isotopic fractionation factors for tropical African plants, we refrained from correcting the δD records for changes in C_3 and C_4 plant contributions.

The observed correlation of depleted δD values of the *n*-C_{31} and *n*-C_{33} alkanes with more enriched $\delta^{13}C$ values, indicating higher C_4 plant contribution, is unexpected as C_4 grasses typically occur under more arid conditions than C_3 plants[13]. Other factors favouring C_4 plants are lower atmospheric CO_2 levels and higher temperatures[13]. CO_2 forcing is, however, ruled out as atmospheric CO_2 levels did not decline during the YD[14]. Air temperature changes may exert a control on C_3/C_4 plant abundances if MBT-derived air temperature estimates reflect a climatic signal and not solely provenance changes of the organic material (see discussion below). Climate-driven long-term vegetation changes likely occurred in the Zambezi catchment. The stronger correlation of the $\delta^{13}C$ values of the *n*-alkanes with their δD values (r^2 = 0.33 for the *n*-C_{31} alkane) than with the air temperature estimates (r^2 = 0.13 for the *n*-C_{31} alkane), however, points to a common hydrologic forcing. We infer that C_4 plant-derived organic material is preferentially derived from the lower Zambezi floodplain under wet conditions, while only C_3 plant-derived organic material is exported from near-coastal vegetation under dry conditions. These provenance changes likely mask any potential long-term vegetation changes.

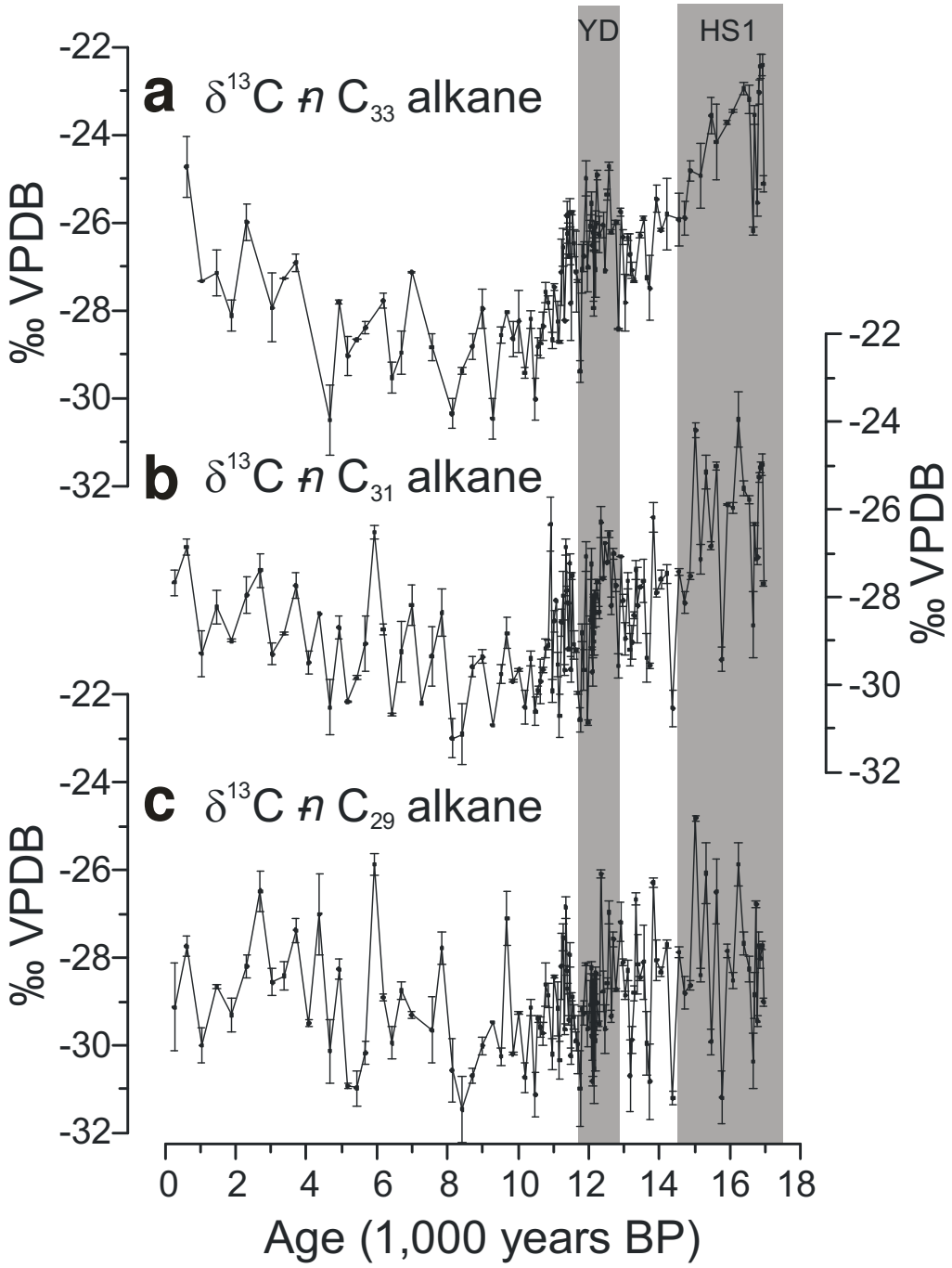

Supplementary Figure S2: Stable carbon isotope compositions of long-chain plant waxes. a, $\delta^{13}C$ of *n*-C_{33} alkane. **b**, $\delta^{13}C$ of *n*-C_{31} alkane. **c**, $\delta^{13}C$ of *n*-C_{29} alkane. Error bars based on replicate analyses. Grey bars indicate intervals of Heinrich Stadial 1 (HS1) and the Younger Dryas (YD).

Regional significance of ocean temperature reconstructions from GeoB9307-3

Alkenone-based SST estimates from GeoB9307-3 could not be obtained due to low abundance of alkenones in the samples. Therefore, TEX_{86}-based[18] temperature estimates were determined. Uncertainty of TEX_{86} measurements is 0.02 based on duplicate analyses of selected samples. The most recent calibration of TEX_{86} to ocean temperature was used[19]. The analytical uncertainty amounts to an absolute error of 0.9°C, smaller than the calibration error. For comparison of the TEX_{86}-based SST record from GeoB9307-3 we use the foraminifera-based SST estimates from core MD79-257 (20°24‘S, 36°20‘E, 1262 m water depth) in the Mozambique Channel[20], which is the only published sediment core SST-record in the vicinity with comparable temporal resolution (Fig. S3). As TEX_{86}-based temperature estimates are thought to reflect mean annual signals, mean annual SSTs from MD79-257 were calculated from warm and cold season estimates[20]. Both records show similar ranges of temperature estimates and parallel changes over the last 17,000 years. Some deviations exist on short time-scales, which might be due to age model uncertainties. Average absolute temperature deviation is 0.7°C between records, within calibration errors of both methods. The high SST in the south-west Indian Ocean during the deglaciation depicted by these records are further supported by warm surface ocean conditions in the western tropical Indian Ocean, the source area of the Mozambique Current[21].

The coherent changes in the temperature records from GeoB9307-3 and MD79-257 suggest that TEX_{86}-based temperature estimates at site GeoB9307-3 reflect SST. The TEX_{86}-based temperature estimates show no correlation with changes in BIT index ($r^2 = 0.13$). This suggests that TEX_{86}-based temperature estimates of

GeoB9307-3 are not biased by the high BIT values in parts of the record[22]. This observation is in accordance with the suggestion that TEX_{86}-based temperatures will be biased by land-derived glycerol-dialkyl-glycerol-tetraether contributions when air temperatures are high relative to ocean temperatures[22] which is not the case for this setting. Additionally, the observed temperature range (25-29°C) in our record strongly resembles the range of TEX_{86}-based temperature estimates observed in core MD96-2048 (26°10‘S, 34°01‘E, 660 m water depth) off the Limpopo showing consistently low BIT indices[23]. Unlike the alkenone-based SST estimates from MD79-257[24], which were inferred to be influenced by strong lateral transport in the Mozambique Current[20], TEX_{86}-based SST estimates of GeoB9307-3 are thought to reflect conditions at the core site as this location is morphologically protected from the Mozambique Current due to its near coastal setting.

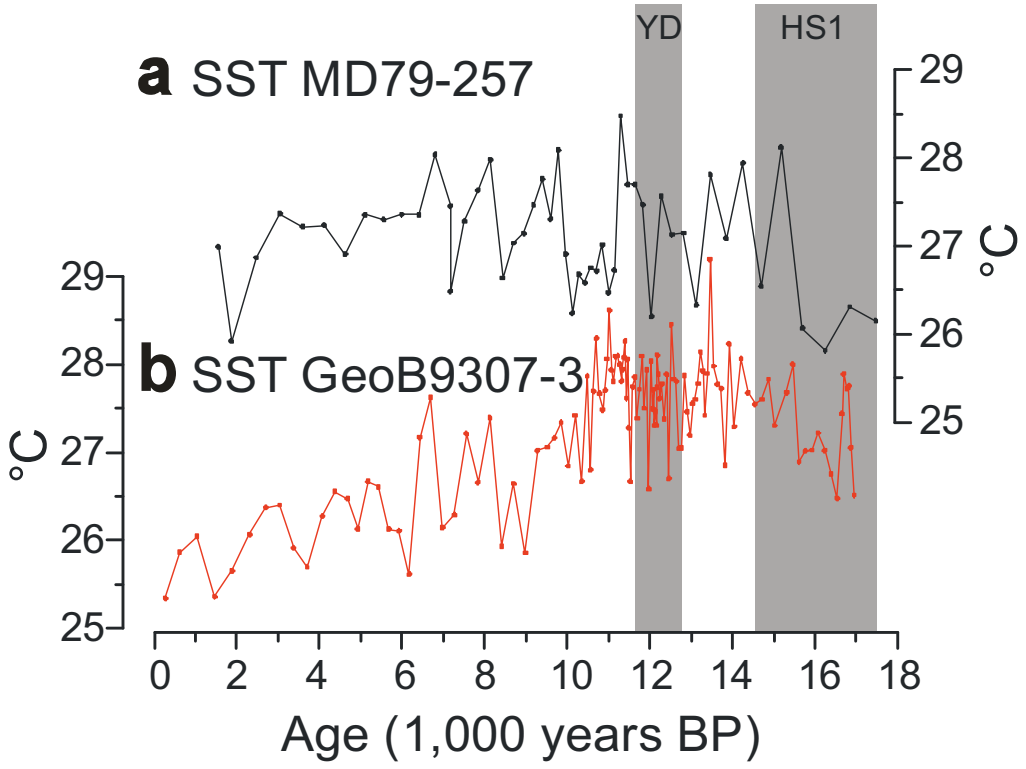

Supplementary Figure S3: Southwest Indian Ocean temperature records. a, Annual SST of core MD79-257 based on averaging of cold- and warm season foraminiferal SST estimates[20]. **b**, TEX_{86}-based SST estimates of GeoB9307-3. Note that Y-scales are equal but offset for comparison. Grey bars indicate intervals of Heinrich Stadial 1 (HS1) and the Younger Dryas (YD).

Air temperature and soil pH reconstructions from GeoB9307-3

Next to TEX_{86} and BIT analyses (BIT shown in Fig. 2c, precision of BIT analyses 0.02 based on duplicate analyses of selected samples) the cyclisation ratio (CBT) and the methylation index (MBT) of the branched tetraethers were determined. Based on duplicate analyses of selected samples, uncertainties of CBT and MBT analyses are 0.09 and 0.03, respectively. Variations in CBT are thought to relate to soil pH changes and variations in MBT to mean annual air temperature changes (MAAT)[15]. Errors of air temperature and soil pH estimates amount to 0.8°C and 0.2 pH units, both much smaller than calibration errors[15]. Soil pH estimates strongly co-vary with changes in the BIT index (Fig. S4). As soil pH changes are mainly driven by variable rainfall amounts due to soil leaching[16], the reconstructed soil pH changes provide strong support to the inferred rainfall changes based on elemental data, BIT indices, sedimentary *n*-alkane concentrations and *n*-alkane isotopic compositions. The global soil calibration[15], however, results in too low air temperature estimates (14°C) for the core-top sample when compared to modern climatological data (University of Delaware data set, http://climate.geog.udel.edu/~climate/). The offset to modern MAAT amounts to about 10°C. A similar offset in MBT-reconstructed MAAT estimates has been observed for water-saturated soils in Uganda[17]. We therefore suggest that the global MBT-MAAT soil calibration may not be applicable to the lower Zambezi catchment likely due to specific local soil conditions and characteristics. If relative changes in MAAT estimates are considered, the reconstructed air temperatures follow SST estimates from GeoB9307-3. Warmest temperatures are reconstructed for the YD with slightly colder conditions during HS1. In the Holocene, lower temperatures persisted with a sudden drop in temperatures between 9,000 and

7,000 years ago. This suggests that air temperatures in the lower Zambezi catchment principally follow SST changes. Source area changes due to relative contribution changes between floodplain and coastal areas, however, might interfere. Under wetter conditions, when more soil organic material from the floodplain is exported, MAAT estimates show higher values than under drier conditions when only coastal areas are exporting soil organic matter with a colder signature. Possibly thus, provenance changes in soil organic matter origin superimpose the climatic temperature evolution in the lower Zambezi catchment reconstructed by MBT-MAAT estimates.

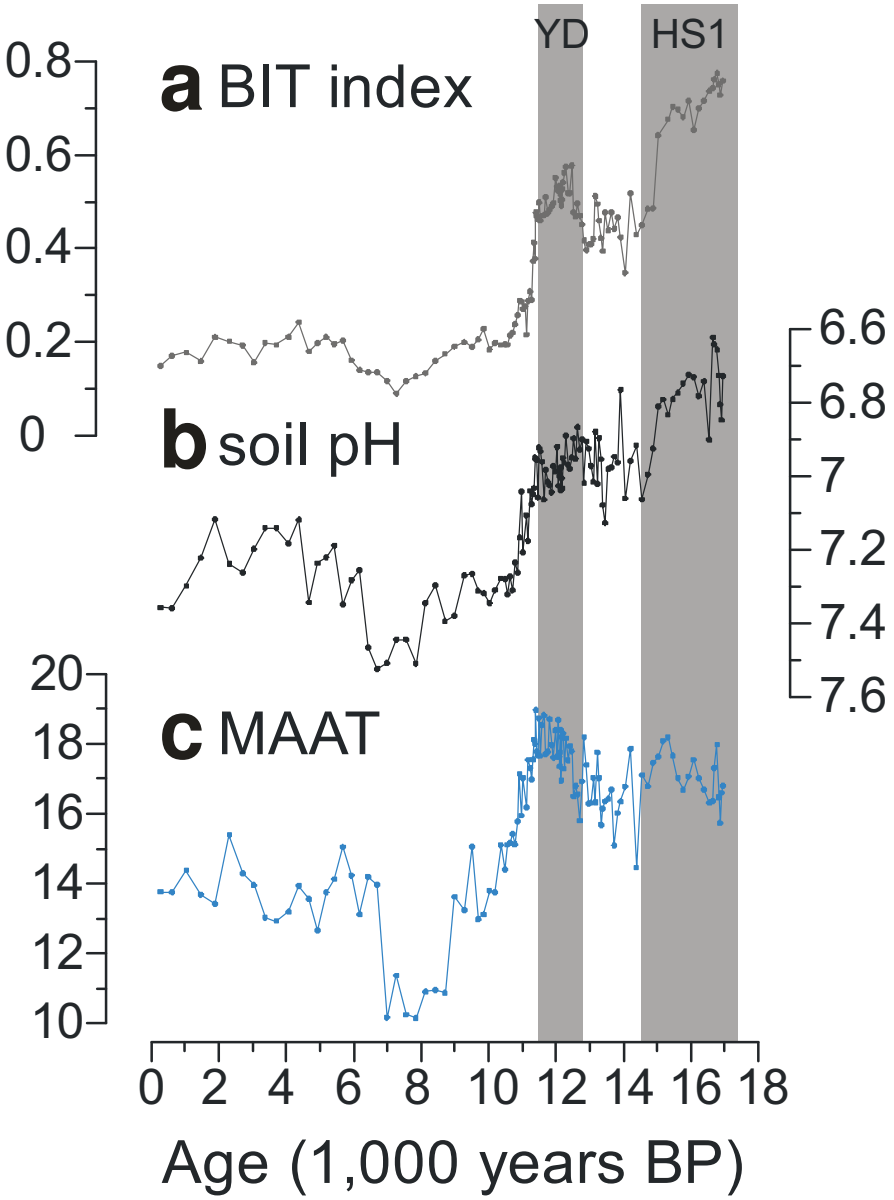

Supplementary Figure S4: Tetraether-based proxy records for soil organic matter contributions, soil pH, and mean annual air temperature (MAAT). **a**, relative soil organic matter contributions based on BIT index[28]. **b**, soil pH estimates based on CBT ratio[15]. **c**, MAAT estimates based on the MBT index[15]. Soil pH and MAAT estimates based on the global soil calibration[15]. Grey bars indicate intervals of Heinrich Stadial 1 (HS1) and the Younger Dryas (YD).

Table S1: ^{14}C-AMS dates used for the chronology of GeoB9307-3

Sample	Core depth (cm)	^{14}C age (^{14}C years)	Error (^{14}C years)	Calendar age range (1σ) (years)
KIA 28442	3	930	30	398-483
KIA 28441	28 294	5 45		2477-2661
KIA 28440	58 455	5 35		4500-4651
KIA 28438	98 629	0 50		6508-6651
KIA 28437	148	8910	55	9396-9503
KIA 28436	178	9730	60	10385-10535
KIA 28435	208	10075	60	10760-11035
KIA 28434	248	10470	60	11206-11406
KIA 28431	283	10570	60	11348-11661
KIA 28430	333	10840	60	11941-12194
KIA 28429	378	10920	70	12073-12353
KIA 28428	413	11220	70	12545-12675
KIA 27758	458	11870	80	13132-13283
KIA 27757	478	12140	90	13322-13513
KIA 27755	508	12680	90	13855-14092
KIA 27754	533 131	20 100		14546-15091
KIA 27753	558 135	30 100		15189-15911
KIA 27752	593 140	20 120		16443-16830
KIA 27751	633 144	50 110		16846-17098

Conversion of radiocarbon ages to calendar ages was done using the program Calib 6.0.1[25] and the Marine09 calibration curve[26]. A regional reservoir age offset of +140±25 years was applied[27]. Ages were linearly interpolated between mean points of age ranges.

References

1 Eglinton, G. and Hamilton, R.J., Leaf epicuticular waxes. *Science* **156**, 1322 (1967).

2 Rommerskirchen, F. et al., Chemotaxonomic significance of distribution and stable carbon isotopic composition of long-chain alkanes and alkan-1-ols in C-4 grass waxes. *Organic Geochemistry* **37** (10), 1303 (2006); Vogts, A., Moossen, H., Rommerskirchen, F., and Rullkötter, J., Distribution patterns and stable carbon isotopic composition of alkanes and alkan-1-ols from plant waxes of African rain forest and savanna C-3 species. *Organic Geochemistry* **40** (10), 1037 (2009).

3 Ficken, K. J., Li, B., Swain, D. L., and Eglinton, G., An n-alkane proxy for the sedimentary input of submerged/floating freshwater aquatic macrophytes. *Organic Geochemistry* **31** (7-8), 745 (2000); Mead, R., Xu, Y. P., Chong, J., and Jaffe, R., Sediment and soil organic matter source assessment as revealed by the molecular distribution and carbon isotopic composition of n-alkanes. *Organic Geochemistry* **36** (3), 363 (2005); Versteegh, G. J. M. et al., Taraxerol and Rhizophora pollen as proxies for tracking past mangrove ecosystems. *Geochimica et Cosmichimica Acta* **68** (3), 411 (2004).

4 Rao, Z. G. et al., Compound specific delta D values of long chain n-alkanes derived from terrestrial higher plants are indicative of the delta D of meteoric waters: Evidence from surface soils in eastern China. *Organic Geochemistry* **40** (8), 922 (2009); Sachse, D. , Radke, J., and Gleixner, G., Hydrogen isotope ratios of recent lacustrine sedimentary *n*-alkanes record modern climate variability. *Geochimica et Cosmochimica Acta* **68**, 4877 (2004); Sachse, D., Radke, J., and Gleixner, G., dD values of individual n-alkanes from terrestrial plants along a climatic gradient - Implications for the sedimentary biomarker record. *Organic Geochemistry* **37**, 469 (2006); Tierney, J. E., Russell, J. M., and Huang, Y. S., A molecular perspective on Late Quaternary climate and vegetation change in the Lake Tanganyika basin, East Africa. *Quaternary Science Reviews* **29** (5-6), 787 (2010).

5 Gat, J. R., Oxygen and hydrogen isotopes in the hydrologic cycle. *Annual Review of Earth and Planetary Sciences* **24**, 225 (1996).

6 Schrag, D. P. et al., The oxygen isotopic composition of seawater during the Last Glacial Maximum. *Quaternary Science Reviews* **21** (1-3), 331 (2002).

7 Gimeno, L. et al., On the origin of continental precipitation. *Geophysical Research Letters* **37**, L13804 (2010).

8 Risi, C., Bony, S., and Vimeux, F., Influence of convective processes on the isotopic composition (delta(18)O and delta D) of precipitation and water vapor in the tropics: 2. Physical interpretation of the amount effect. *J. Geophys. Res.-Atmos.* **113** (D19) (2008); Risi, C. et al., What controls the isotopic composition of the African monsoon precipitation? Insights from event-based precipitation collected during the 2006 AMMA field campaign. *Geophys. Res. Lett.* **35** (24) (2008).

9 Frankenberg, C. et al., Dynamic Processes Governing Lower-Tropospheric HDO/H(2)O Ratios as Observed from Space and Ground. *Science* **325** (5946), 1374 (2009).

10 Ehleringer, J.R. and Cerling, T.E., in *Encyclopedia of Global Environmental Change*, edited by T. Munn (John Wiley & Sons, Ltd, Chichester, 2002), Vol. 2, pp. 186.

11 Castaneda, I. S. et al., Wet phases in the Sahara/Sahel region and human migration patterns in North Africa. *Proceedings of the National Academy of Sciences* **106** (48), 20159 (2009).

12 Hou, J. Z., D'Andrea, W. J., MacDonald, D., and Huang, Y. S., Hydrogen isotopic variability in leaf waxes among terrestrial and aquatic plants around Blood Pond, Massachusetts (USA). *Organic Geochemistry* **38** (6), 977 (2007).

13 Collatz, G.J., Berry, J.A., and Clark, J.S., Effects of climate and atmospheric CO_2 partial pressure on the global distribution of C_4 grasses: present, past and future. *Oecologia* **114**, 441 (1998).

14 Blunier, T. et al., Timing of the Antarctic cold reversal and the atmospheric CO_2 increase with respect to the Younger Dryas event. *Geophysical Research Letters* **24** (21), 2683 (1997).

15 Weijers, J. W. H. et al., Environmental controls on bacterial tetraether membrane lipid distribution in soils. *Geochimica et Cosmochimica Acta* **71** (3), 703 (2007).

16 Johnson, D. W. et al., Precipitation change and soil leaching: Field results and simulations from Walker Branch Watershed, Tennessee. *Water, Air, & Soil Pollution* **105** (1-2), 251 (1998).

17 Loomis, S.E., Russell, J. M., and Sinninghe Damsté, J. S., Distributions of branched GDGTs in soils and lake sediments from western Uganda: Implications for a lacustrine paleothermometer. *Organic Geochemistry* **42**, 739 (2011).

18 Schouten, S., Hopmans, E.C., Schefuß, E., and Sinninghe Damsté, J.S., Distributional variations in marine crenarcheotal membrane lipids: a new tool for reconstructing ancient sea water temperatures? *Earth and Planetary Science Letters* **204**, 265 (2002).

19 Kim, J. H. et al., New indices and calibrations derived from the distribution of crenarchaeal isoprenoid tetraether lipids: Implications for past sea surface temperature reconstructions. *Geochimica et Cosmichimica Acta* **74** (16), 4639 (2010).

20 Levi, C. et al., Low-latitude hydrological cycle and rapid climate changes during the last deglaciation. *Geochemistry Geophysics Geosystems* **8**, doi:10.1029/2006GC001514 (2007).

21 Kiefer, T., McCave, I. N., and Elderfield, H., Antarctic control on tropical Indian Ocean sea surface temperature and hydrography. *Geophysical Research Letters* **33** (24) (2006).

22 Weijers, J.W.H., Schouten, S., Spaargaren, O.C., and Sinninghe Damste, J.S., Occurrence and distribution of tetraether membrane lipids in soils: Implications for the use of the TEX_{86} proxy and the BIT index. *Organic Geochemistry* **37**, 1680 (2006).

23 Caley, T. et al., High-latitude obliquity forcing drives the Agulhas leakage. *Climate of the Past Discussions* **7**, 2193 (2011).

24 Bard, E. , Rostek., F., and Sonzogni, C., Interhemispheric synchrony of the last deglaciation inferred from alkenone paleothermometry. *Nature* **385**, 707 (1997).

25 Stuiver, M. and Reimer, P.J., Extended ^{14}C data base and revised CALIB 3.0 ^{14}C age calibration program. *Radiocarbon* **35**, 215 (1993).

26 Reimer, P. J. et al., IntCal09 and Marine09 Radiocarbon Age Calibration Curves, 0-50,000 Years cal BP. *Radiocarbon* **51** (4), 1111 (2009).

27 Southon, J. et al., Marine reservoir corrections for the Indian Ocean and southeast Asia. *Radiocarbon* **44** (1), 167 (2002).

28 Hopmans, E.C., Schefuß, E., Sinninghe Damsté, J.S., and Schouten, S., A novel proxy for terrestrial carbon input based on branched and isoprenoid tetraethers. *Earth and Planetary Science Letters* **224**, 107 (2004).